Bioorg. Med. Chem. Lett. 34 (2021) 127759

Contents lists available at ScienceDirect

Bioorganic & Medicinal Chemistry Letters

journal homepage: www.elsevier.com/locate/bmcl

Novel amide and imidazole compounds as potent hematopoietic prostaglandin D_2 synthase inhibitors

Kirk L. Olson *, Melissa C. Holt, Fred L. Ciske, James B. Kramer, Paige E. Heiple, Margaret L. Collins, Carrie M. Johnson, Chi S. Ho, M. Ines Morano, Stephen D. Barrett

Cayman Chemical Company, Inc., 1180 East Ellsworth Rd., Ann Arbor, MI, USA

ARTICLE INFO

Keywords:
Hematopoietic D_2 synthase
H-PGDS
Prostaglandin D_2
PGD_2
Structure-activity-relationship
SAR

ABSTRACT

In seeking novel and potent small molecule hematopoietic prostaglandin D_2 synthase (H-PGDS) inhibitors as potential therapies for PGD_2-mediated diseases and conditions, we explored a series comprising multiple aryl/heteroaryl rings attached in a linear arrangement. Each compound incorporates an amide or imidazole "linker" between the pyrimidine or pyridine "core" ring and the "tail" ring system. We synthesized and screened twenty analogs by fluorescence polarization binding assay, thermal shift assay, glutathione *S*-transferase inhibition assay, and a cell-based assay measuring suppression of LPS-induced PGD_2 stimulation. Amide analogs show ten-fold greater shift in the thermal shift assay in the presence of glutathione (GSH) versus the same assay run in the absence of GSH. The imidazole analogs did not produce a significant change in thermal shift between the two assay conditions, suggesting a possible stabilization effect of the amide linker in the synthase-GSH-inhibitor complex. Imidazole analog **23**, **(KMN-010034)** demonstrates superior potency across the *in vitro* assays and good *in vitro* metabolic stability in both human and guinea pig liver microsomes.

Introduction

Prostaglandin D_2 (PGD_2) is released in large quantities during allergic and asthmatic anaphylaxis from activated mast cells, reaching levels 100–1000 times higher than those produced by platelets, macrophages, *T*-helper and dendritic cells.[1] PGD_2 also plays a detrimental pro-inflammatory role in systemic mastocytosis, rheumatoid arthritis, and Duchenne's muscular dystrophy.[2,3] PGD_2 synthesis from the cyclic endoperoxide arachidonic acid (AA) metabolite, prostaglandin H_2 (PGH_2), is catalyzed by two enzymes, lipocalin-type PGD_2-synthase (L-PGDS) and hematopoietic-type PGD-synthase (H-PGDS) (Scheme 1).[4–6] L-PGDS expression is largely localized to the brain, whereas H-PGDS expression occurs primarily within the peripheral tissues.[6] PGD_2 is the endogenous activating ligand for two prostaglandin receptors, PGD_2 receptor 1 (DP_1) and PGD_2 receptor 2 (DP_2 or $CRTH_2$), where these receptors mediate complex downstream effects which can be pro-inflammatory or anti-inflammatory in various instances.[7,8] H-PGDS is therefore a central protein target for development of selective, potent inhibitors for therapeutic use against PGD_2-mediated diseases and conditions.

H-PDGS is a sigma-type glutathione transferase that catalyzes the bi-bi molecular reaction between nucleophilic cofactor glutathione (GSH) and electrophilic substrate PGH_2. HQL-79 (Fig. 1) was among the first-generation human H-PGDS inhibitors identified. HQL-79 inhibits H-PGDS competitively with PGH_2 and possesses moderate potency with a K_i of 5 μM.[9] Surface plasmon resonance (SPR) revealed that HQL-79 bound H-PGDS with 12-fold higher affinity in the presence of GSH and Mg^{2+} than in their absence, supporting that HQL-79 binding is stabilized by enzyme-cofactor-inhibitor interactions, perhaps by a network of hydrogen bonds.[9]

GlaxoSmithKline, Sanofi, Evotec, Pfizer, Asahi Kasei, and AstraZeneca have investigated H-PGDS as a therapeutic target.[3,9–17] Fig. 1 displays some of the compound leads generated from the pharma programs. Though potencies have attained the low- to sub-nM IC_{50} range, none has advanced through FDA approval. Structural similarities between the program leads are evident with most inhibitors having a high degree of aromaticity. The structures mainly comprise three components, an aromatic head group, a linker moiety (often an amide), and a tail portion. Compound **7**, developed by Sanofi, incorporates a 5-(2-hydroxypropan-2-yl)-1,2,4-oxadiazol-3-yl)-phenyl tail moiety, wherein the oxadiazole ring imparts improved metabolic stability benefits over unsubstituted and other substituted phenyl tail group-bearing analogs.[16,17]

We sought to optimize the physicochemical and pharmacokinetic properties of a series of multiheteroaryl H-PGDS inhibitors disclosed from our previous work.[18] These predecessor inhibitors bear similarity to Pfizer and Sanofi H-PGDS inhibitors **3** and **6**, respectively.

* Corresponding author.
E-mail address: kolson@caymanchem.com (K.L. Olson).

https://doi.org/10.1016/j.bmcl.2020.127759
Received 26 October 2020; Received in revised form 17 December 2020; Accepted 20 December 2020
Available online 29 December 2020

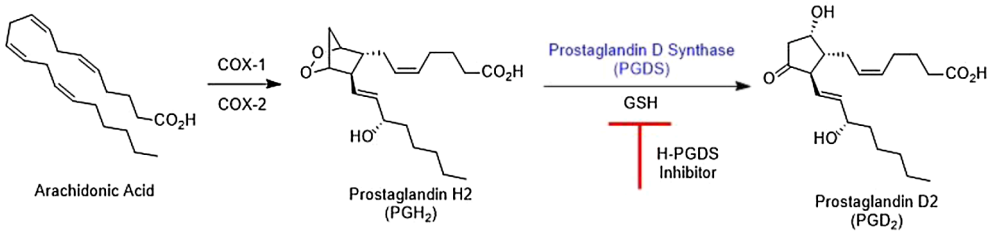

Scheme 1. Arachidonate cyclooxygenase pathway formation of PGD_2.

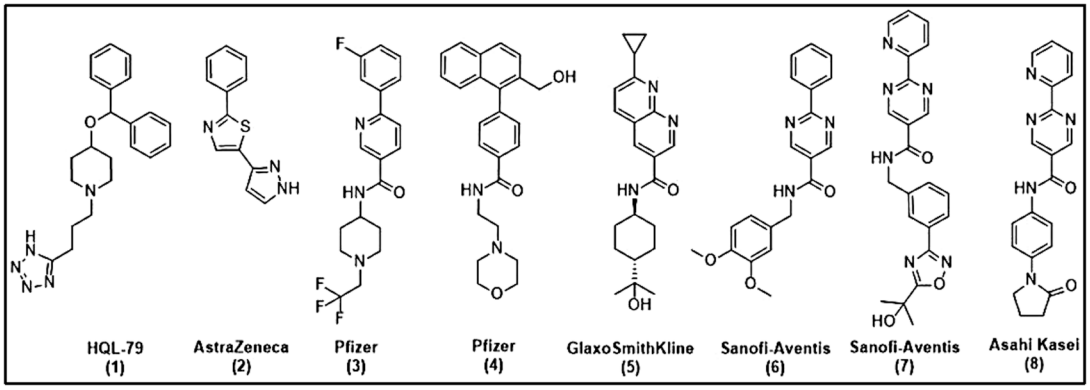

Fig. 1. Examples of known H-PGDS inhibitors.

Compounds of this series comprise a string of covalently linked aromatic rings, including sequentially a phenyl or pyridyl "head" ring, a pyrimidine or pyridine "core" ring, a "linker" 5-membered heterocyclic ring in place of the published amide linker, and a "tail" group typically comprising a pyridine, substituted phenyl, or unsubstituted phenyl ring. We explored the potential of the 5-membered heterocyclic ring linkers, such as imidazole and thiazole, to eliminate the possibility of amidase-mediated hydrolytic cleavage pathway of metabolism. We found the imidazole linkers in place of amide maintained the high potencies of the amide series, though we observed no benefit to solubility or metabolic stability.[18] In this work we generated a series of 20 new multiheteroaryl analogs consisting of various combinations of head-core-linker-tail while incorporating or not incorporating the 5-(2-hydroxypropan-2-yl)-1,2,4-oxadiazol-3-yl in the tail moiety (Table 1). We prepared amide linker-bearing and parallel imidazole linker-bearing analogs to assess impact of this difference on activity profiles.

We constructed the new amide and imidazole analogs using the routes illustrated in Schemes 2–8. Various head ring-core ring combinations are commercially available as carboxylic acid intermediates, including 6-phenylnicotinic acid (**9a**), 2,2′-bipyridine-5-carboxylic acid (**10a**), 2-pyridin-2-ylpyrimidine-5-carboxylic acid (**11a**), and 2-phenyl-5-pyrimidinecarboxylic acid (**12a**). We employed two strategies for preparing the amide analogs. Direct amide coupling with benzylamine provides amide linker-bearing compounds **9**–**12** (Scheme 2).

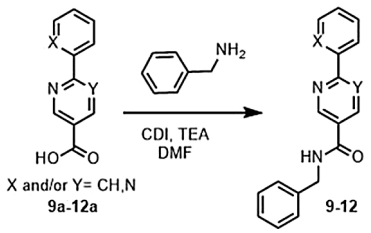

Scheme 2. Synthesis of analogs **9**–**12.**

We approached the amide linker-phenyl-oxadiazole-isopropanol-tail combination through the synthetic construction of the tail, following a published method.[16,17] Subsequent amide coupling to the various commercially available head groups affords compounds **7**, **13**, **14**, and **15** (Scheme 3).

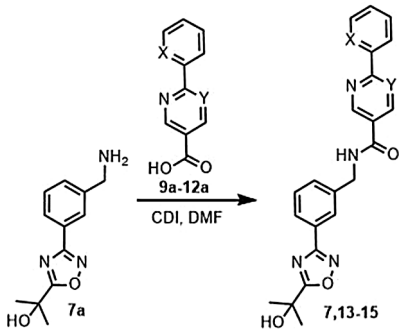

Scheme 3. Synthesis of analogs **7**, **13**–**15.**

For the imidazoles, Weinreb amide activation of the head-core-carboxylic acid intermediates followed by methyl lithium addition provided the key ketone intermediates (Scheme 4). The head-core-methyl ketone intermediates were subsequently brominated using tetrabutylammonium tribromide, forming the α-bromo ketone intermediate. Reaction of the α-bromo ketone intermediates with benzamidine provided compounds **16**, **17**, **18**, and **19.** Phenyl-pyrimidyl intermediate (**19c)** served as the key intermediate for the synthesis of many of the compounds in Table 1, including the 3-pyridyl imidazole analog **24**, and the 3-pyridyl thiazole analog **25**.

Reacting the α-bromo ketones (**16c**, **17c**, and **19c)** with 3-cyanobenzamidine provided a handle for synthesis of the tail region for compounds **20**, **21**, and **23** (Scheme 5). The cyano intermediates were converted to *N*-hydroxybenzimidamides **20b, 21b,** and **23b**, which were subsequently cyclized in a base catalyzed reaction with 2-acetoxyisobutyryl chloride, resulting in the formation of the protected 1,2,4-oxadiazole ring, providing the tail intermediates **20c-23c**. Finally, removal of the acetyl ester afforded compounds **20**–**23**.

Formation of the α-bromo ketone was typically very low yielding for the pyridyl-pyrimidine head group series when using the method in Scheme 5. Consequently, an alternative route towards the α-bromo ketone was employed to generate final analog **22** (Scheme 6). Suzuki-

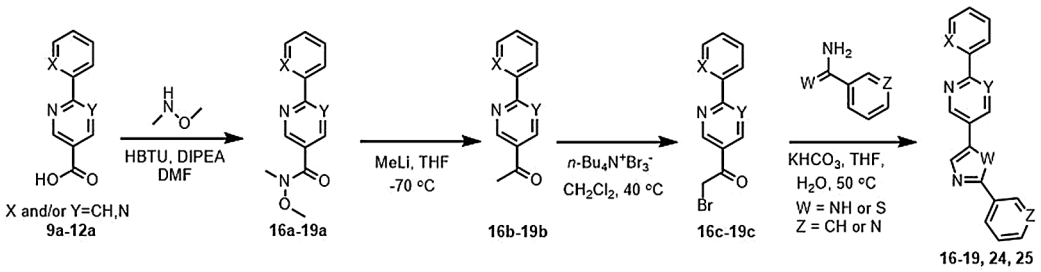

Scheme 4. Synthesis of analogs **16**–**19, 24** and **25.**

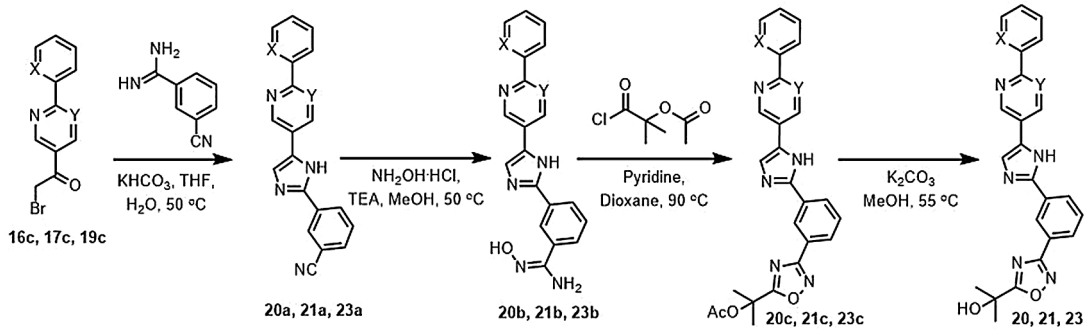

Scheme 5. Synthesis of analogs **20, 21** and **23.**

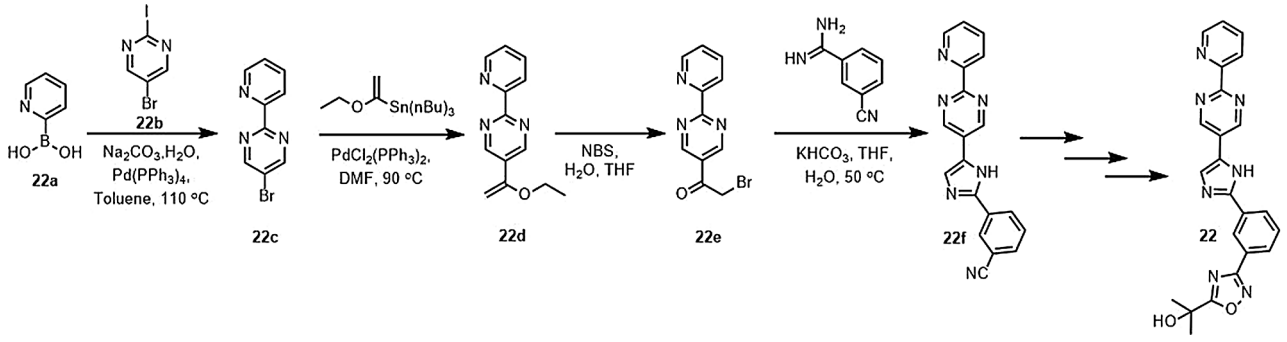

Scheme 6. Synthesis of analog **22.**

Miyaura coupling between the pyridine-2-boronic acid (**22a**) and 5-bromo-2-iodopyrimidine (**22b**) provided intermediate 5-bromo-2-(pyridin-2-yl)pyrimidine (**22c**). Subjection of **22c** to Stille conditions afforded the vinyl ether, which is readily brominated with *N*-bromosuccinimide. Formation of the imidazole through reaction with benzamidine yields **22f.** Likewise, the tail region of **22** is assembled in an identical fashion to that which is depicted in Scheme 5.

Methyl substitution of the imidazole linker ring required alternate synthetic routes (Schemes 7 and 8). Commercially available 4-methyl-2-phenyl-1*H*-imidazole (**26a**) was benzyl-protected at the imidazole *N*1 position. Palladium catalyzed direct arylation between imidazole **26b** and commercially available 5-bromo-2-phenylbromide (**26c)** affords **26d**. Deprotection of **26d** by hydrogenation yielded analog **26**.

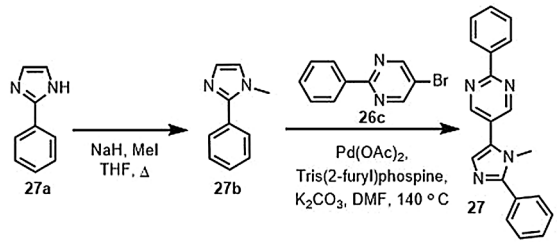

Scheme 8. Synthesis of analog **27.**

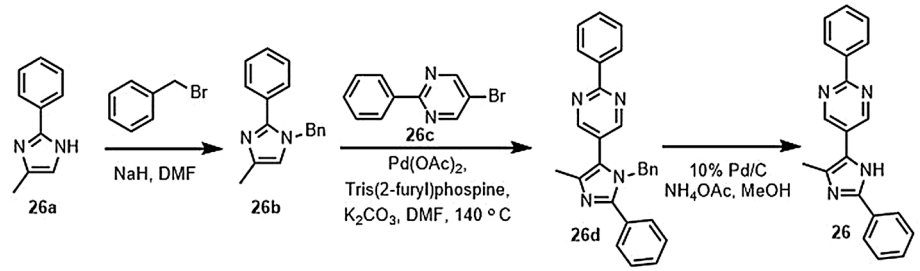

Scheme 7. Synthesis of analog **26.**

The synthesis of 1-methyl substituted imidazole analog **27** is shown in Scheme 8. 1-Methyl-2-phenyl-1*H*-imidazole (**27b**) was obtained via direct methylation of 2-phenyl-1*H*-imidazole (**27a**) with iodomethane. Palladium catalyzed direct arylation between imidazole **27b** and **26c** afforded **27**.

Overall, synthesized analogs in this data set compared individual effects of head-core-linker-tail modifications on activity profiles with the goal to develop potent, and metabolically stable lead H-PGDS inhibitor2s.

Compound screening was performed in a multi-assay format to reduce the risk of false positives and negatives, with the results displayed in Table 1. Overall, the screening paradigm grouped together a competitive binding assay (fluorescence polarization binding assay, FP), a direct-binding assay (TSA/ThermoFluor), a kinetic inhibition assay (GSTase), and a cell-based assay (suppression of LPS-induced PGD_2 stimulation, PGD_2 levels measured by ELISA). Rank-order of compounds was performed using FP derived IC_{50}, melting temperature shift (ΔT_m,

Table 1

SAR of compounds 7, 9–27. FP binding assay IC_{50} and CBA IC_{50} values were calculated using nonlinear regression in GraphPad Prism 7.02 software and are presented as mean ± SEM of (n replicates). ND refers to values that were not determined. Statistical analysis was performed using one-way ANOVA controlling false-discovery rate of multiple comparisons using two-stage linear procedure by Benjamini, Krieger, and Yekutieli. Superscripts indicate that $P < 0.05$ for comparisons with the following compounds 9 (a), 10 (b), 11 (c), 12 (d), 13 (e), 14 (f), 7 (g), 15 (h), 16 (i), 17 (j), 18 (k), 19 (l), 20 (m), 21 (n), 22 (o), 23 (p), 24 (q), 25 (r), 26 (s), 27(t). Compounds which significantly violated the sphericity assumption were excluded from statistical analysis including 18, 22 from FP statistics and 22 from CBA statistics. Statistics are provided for compounds with > 80% inhibition in GSTase assay as well.

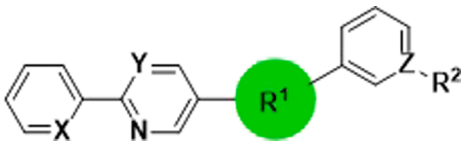

No.	X	Y	R^1	Z	R^2	FP IC_{50} (nM)	ΔT_m (°C)	ΔT_m (°C) w/ 1 mM GSH	% GSTase Inhibition	CBA IC_{50} (nM)
(9)	C	C		C	H	122 ± 51.2 (6)[c-j,l,m,p,q-s]	0.3 ± 0 (3)	3.0 ± 0 (3)	40.4 ± 1.06 (3)	1,234 ± 151 (4)[b-*n*,p,q,s,*t*]
(10)	N	C		C	H	80.7 ± 11.7 (6)[c,d,g,h,l,p,r]	0.1 ± 0.1 (3)	2.8 ± 0.2 (3)	19.2 ± 1.62 (3)	452.8 ± 118.2 (4)[a,c-e,g-*n*,p,q,s]
(11)	N	N		C	H	7.14 ± 2.06 (7)[a,b,*n*,r]	0.2 ± 0.1 (3)	4.2 ± 0 (3)	71.3 ± 1.91 (3)	35.71 ± 4.21 (7)[a,b,e,f,k,s,*t*]
(12)	C	N		C	H	11.7 ± 1.50 (13)[a,b,*n*,r]	0.4 ± 0.1 (3)	4.6 ± 0.1 (3)	82.5 ± 0.51 (3)[g,i,l,p]	23.91 ± 8.53 (11) [a,b,e,f,k,s,*t*]
(13)	C	C		C	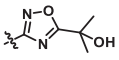	27.7 ± 4.32 (5)[a,r]	0.2 ± 0.1 (3)	3.3 ± 0 (3)	62.4 ± 0.58 (3)	807.75 ± 84.99 (4)[a-d,f-*n*,p,q,s]
(14)	N	C		C	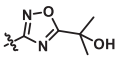	55.5 ± 17.1 (6)[a,p,r]	0.1 ± 0.1 (3)	2.8 ± 0.1 (3)	47.2 ± 6.48 (3)	327.75 ± 41.02 (4)[a,c-e,g,h,k,*n*,p,s,*t*]
(7)	N	N		C	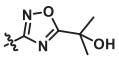	7.48 ± 1.53 (5)[a,b,*n*,r]	0.5 ± 0.1 (3)	5.1 ± 0 (3)	90.9 ± 1.33 (3)[d,h,l,m,s]	11.61 ± 1.67 (10)[a,b,e,f,k,s,*t*]
(15)	C	N		C	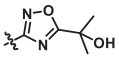	7.18 ± 1.56 (9)[a,b,*n*,r]	0.4 ± 0.1 (3)	4.95 ± 0.15 (3)	83.9 ± 0.61 (3)[g,l,p,s]	9.86 ± 1.54 (16)[a,b,e,f,k,s,*t*]
(16)	C	C		C	H	31.6 ± 10.3 (6)[a,r]	3.2 ± 0.1 (3)	4.4 ± 0.1 (3)	85.2 ± 0.20 (3)[d,g,l,m,p,s]	40.5 ± 2.1 (4)[a,b,e,k,s,*t*]
(17)	N	C		C	H	37.2 ± 6.31 (5)[a,r]	4.2 ± 0 (3)	5.2 ± 0.1 (3)	73.5 ± 4.26 (3)	44.5 ± 12.7 (4)[a,b,e,k,s,*t*]
(18)	N	N		C	H	1,765 ± 1,179 (2)	0.2 ± 0.1 (3)	0.6 ± 0 (3)	18.2 ± 0.47 (3)	5,056 ± 622.7 (4)[a-j,l-*n*,p,q,s,*t*]
(19)	C	N		C	H	8.88 ± 2.9 (9)[a,b,*n*,r]	3.6 ± 0 (3)	3.8 ± 0.1 (3)	94.5 ± 0.31 (3)[d,g,h,i,m,p,s]	59.00 ± 12.16 (6)[a,b,e,k,s,*t*]
(20)	C	C		C	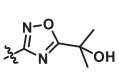	35.4 ± 17.3 (3)[a,r]	4.3 ± 0.1 (3)	5.2 ± 0.1 (3)	83.5 ± 0.29 (3)[g,i,l,p,s]	72.0 ± 14.13 (7)[a,b,e,k,s,*t*]
(21)	N	C		C	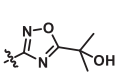	78.6 ± 18.3 (6)[c,d,g,h,l,r]	4.8 ± 0 (3)	5.4 ± 0 (3)	76.1 ± 4.62 (3)	23.41 ± 5.68 (7)[a,b,e,f,k,s,*t*]
(22)	N	N		C	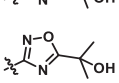	3,203 ± 1,214 (3)	0.4 ± 0.1 (3)	0.6 ± 0 (3)	25.5 ± 14.9 (3)	ND
(23)	C	N		C	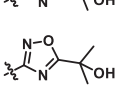	5.88 ± 1.18 (15)[a,b,f,*n*,r,*t*]	6.9 ± 0.1 (3)	7.1 ± 0.1 (3)	92.1 ± 0.66 (3)[d,h,i,l,m]	20.67 ± 3.38 (18)[a,b,e,f,k,s,*t*]

(*continued on next page*)

Table 1 (*continued*)

No.	X	Y	R^1	Z	R^2	FP IC_{50} (nM)	ΔT_m (°C)	ΔT_m (°C) w/ 1 mM GSH	% GSTase Inhibition	CBA IC_{50} (nM)
(24)	C	N		N		13.2 ± 5.42 (3)[a,r]	4.9 ± 0.1 (3)	5.7 ± 0 (3)	65.1 ± 1.09 (3)	12.5 ± 4.5 (2)[a,b,e,k,s,t]
(25)	C	N		N		257 ± 159 (2)[a-j,l-n,p,q,s,t]	2.1 ± 0 (3)	2.2 ± 0.1 (3)	29.5 ± 1.41 (3)	>5,000 (2)
(26)	C	N		C	H	30.8 ± 10.2 (3)[a,r]	4.3 ± 0.1 (3)	4.5 ± 0 (3)	81.5 ± 0.98 (3)[g,h,i,l,m,p]	3,742.5 ± 338.5 (2)[a-n,p,q,t]
(27)	C	N		C	H	63.1 ± 19.4 (3)[p,r]	3.1 ± 0.1 (3)	3.4 ± 0.1 (3)	38.4 ± 7.8 (3)	723.5 ± 95.5 (2)[a,c,d,f-n,p,q,s]

°C) in the presence/absence of GSH, percent GSTase inhibition, and cell-based assay (CBA) derived IC_{50}.

Analogs bearing the pyrimidine ring core generally excel in H-PGDS binding and cellular potencies over their corresponding pyridine analogs with pyrimidines **23**, **11**, **15**, **7**, **19**, and **12** representing the six most potent compounds of the twenty tested in the FP binding assay, and all these except for **19** representing the five most potent in the CBA (Table 1). The phenyl(head)-pyrimidine(core)-linker-5-(2-hydroxypropan-2-yl)-1,2,4-oxadiazol-3-yl)-phenyl(tail) combination represented by amide linker analog **15** and imidazole linker analog **23** is quite favorable, providing two of the most potent compounds in the FP binding assay, CBA, and GSTase inhibition assay while demonstrating relatively strong shifts in the TSA.

In one of the most clear and dramatic observations of the series SAR, the pyridine-pyrimidine-imidazole-tail group combination as represented by analogs **18** and **22** is detrimental to binding and activity across the panel of assays. Simple replacement of any one of the three nitrogen atoms of the head group-core ring component with a carbon atom (**17**, **19**, **21**, and **23**) restores orders of magnitude to the FP and CBA IC_{50}s while also recovering significant activity in both the TSA and GSTase assay. The detrimental impact of the pyridine-pyrimidine combination on H-PGDS binding and activity is not observed when the linker is the amide, as observed across the assay panel for two sets of compounds **10**-**11**-**12**, and **14**–**17**-**15**. Interestingly, we observed a 10-fold increased TSA shift for all eight amide linker analogs when the assay included a 1 mM concentration of the glutathione cofactor (GSH) over those shifts observed when GSH was not added. The amide core displaying a dependence upon GSH matches broadly with previously reported work showing an enhancement in K_i in the presence of GSH.[9] We did not observe such a change, however, in shift for heterocycle linker analogs. The imidazole linked series displayed nearly an equivalent ΔT_m in the presence or absence of GSH (Fig. 2). This suggests that specific interactions (perhaps hydrogen bonding interactions) between the cofactor and amide group stabilize the cofactor-inhibitor-synthase binding complex. Analog **23** displayed the largest T_m shift in the TSA, 6.9/7.1 °C, in the absence or presence of GSH, relative to all other compounds screened. The observed T_m shift between the amide and imidazole series suggested further study on the mode of inhibition was needed. GSH competitive binding (imidazole series) versus non-competitive binding (amide series) will be further investigated in an upcoming publication.

Analogs **24**-**27** test variations of the 5-membered heterocycle linker-tail group motif while maintaining the phenyl-pyrimidine head group-core ring arrangement. The pyridin-3-yl tail of imidazole analog **24** imparts binding and activity across the assay panel. Replacing the 1-nitrogen atom of imidazole analog **24** with a sulfur atom to provide thiazole analog **25** results in the significant loss of H-PGDS binding potencies and activity, whereas methyl substitutions at various imidazole ring positions (analogs **26** and **27**) slightly diminish binding yet still significantly decrease cell activity.

Lastly, analog **23**, **KMN-010034** showed good *in vitro* stability with a half-life > 60 min when tested in human liver microsomes. Unfortunately, we achieved a maximum aqueous **KMN-010034** concentration of only 3.3 μM in PBS @ pH 7.4. Replacement of the phenyl head ring with 2-pyridyl offers an aqueous solubility benefit. We observed improved solubility for the 2-pyridyl head ring analog of **23**, compound **22**, for which we achieved a maximum aqueous concentration of 17.5 μM under the same conditions.

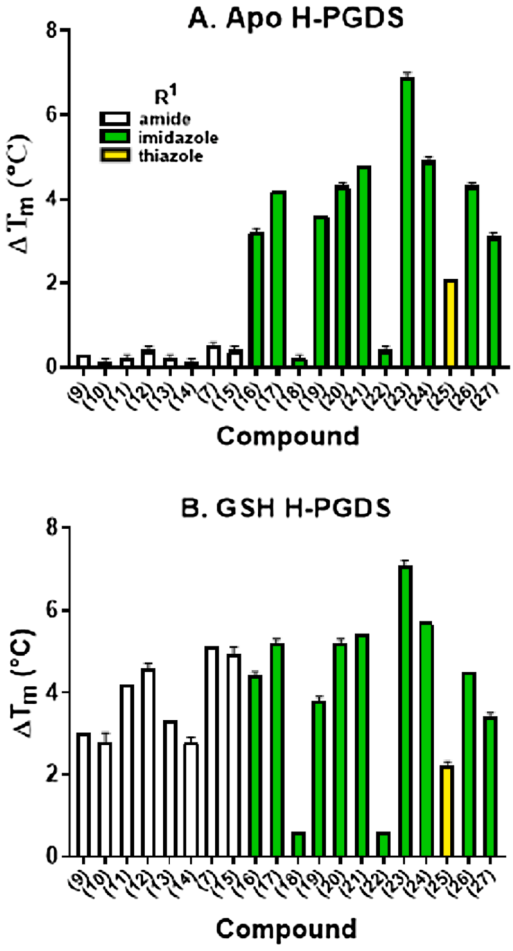

Fig. 2. A) Change in melting temperature observed in TSA to Apo H-PGDS. (B) Change in melting temperature observe in TSA to Apo H-PGDS in the presence of GSH. All error bars are SEM.

Declaration of Competing Interest

The authors declare that they have no known competing financial interests or personal relationships that could have appeared to influence the work reported in this paper.

Acknowledgments

We thank Yoshi Urade for past guidance and insight. We thank former project members for their research and dedication. We would especially like to thank Kirk Maxey for his continued guidance and support. All funds were R&D expenditures of Cayman Chemical Company, Inc.

Appendix A. Supplementary data

Supplementary data to this article can be found online at https://doi.org/10.1016/j.bmcl.2020.127759.

References

1 Bochenek, G., E. Nizankowska, A. et al. Plasma 9alpha, 11beta-PGF2, a PGD2 metabolite, as a sensitive marker of mast cell activation by allergen in bronchial asthma. Thorax 2004;59(6):459-464. http://dx.doi.org/10.1136/thx.2003.013573.
2 Kanaoka Y, Urade Y. Hematopoietic prostaglandin D synthase. *Prostaglandins Leukot Essent Fatty Acids*. 2003;69(2–3):163–167. https://doi.org/10.1016/S0952-3278(03)00077-2.
3 Thurairatnam S. Hematopoietic prostaglandin D synthase inhibitors. *Prog Med Chem*. 2012;51:97–133. https://10.1016/B978-0-12-396493-9.00004-2.
4 Kanaoka Yoshihide, Ago Hideo, Inagaki Eiji, et al. Cloning and crystal structure of hematopoietic prostaglandin D synthase. *Cell*. 1997;90(6):1085–1095. https://doi.org/10.1016/S0092-8674(00)80374-8.
5 Irikura D, Kumasaka T, Yamamoto M, et al. Cloning, expression, crystallization, and preliminary X-ray analysis of recombinant mouse lipocalin-type prostaglandin D synthase, a somnogen-producing enzyme. *J Biochem*. 2003;133(1):29–32. https://doi.org/10.1093/jb/mvg006.
6 Urade Y, Eguchi N. Lipocalin-type and hematopoietic prostaglandin D synthases as a novel example of functional convergence. *Prostag Oth Lipid M*. 2002;68–69:375–382. https://doi.org/10.1016/S0090-6980(02)00042-4.
7 Korbecki J, Baranowska-Bosiacka I, Gutowska I, et al. Cyclooxygenase pathways. *ACTA Biochim Pol*. 2014;61(4):639–649. http://www.actabp.pl/pdf/4_2014/639.pdf.
8 Song W-L, Ricciotti E, Liang X, et al. L-PGDS but not H-PGDS deletion causes hypertension and accelerates thrombogenesis in mice. *J Pharmacol Exp Ther*. 2018;367(3):425–432. https://doi.org/10.1124/jpet.118.250936.
9 Aritake Kosuke, Kado Yuji, Inoue Tsuyoshi, Miyano Masashi, Urade Yoshihiro. Structural and functional characterization of HQL-79, an orally selective inhibitor of human hematopoietic prostaglandin D synthase. *J Biol Chem*. 2006;281(22):15277–15286.
10 Carron Chris P, Trujillo John I, Olson Kirk L, et al. Discovery of an oral potent selective inhibitor of hematopoietic prostaglandin D synthase (HPGDS). *ACS Med Chem Lett*. 2010;1(2):59–63. https://doi.org/10.1021/ml900025z.
11 Aldous, S. C., Jiang, J. Z., Lu, J. et al. Preparation of pyrimidine amide derivatives as prostaglandin D synthase inhibitors. WO2007041634 A1, 2007.
12 Trujillo John I, Kiefer James R, Huang Wei, et al. Investigation of the binding pocket of human hematopoietic prostaglandin (PG) D2 synthase (hH-PGDS): a tale of two waters. *Bioorg Med Chem Lett*. 2012;22(11):3795–3799. https://doi.org/10.1016/j.bmcl.2012.04.004.
13 Hohwy Morten, Spadola Loredana, Lundquist Britta, et al. Novel prostaglandin d synthase inhibitors generated by fragment-based drug design. *J Med Chem*. 2008;51(7):2178–2186. https://doi.org/10.1021/jm701509k.
14 Cadilla Rodolfo, Deaton David N, Do Young, et al. The exploration of aza-quinolines as hematopoietic prostaglandin D synthase (H-PGDS) inhibitors with low brain exposure. *Bioorg Med Chem*. 2020;28(23):115791. https://doi.org/10.1016/j.bmc.2020.115791.
15 Takaya Daisuke, Inaka Koji, Omura Akifumi, et al. Characterization of crystal water molecules in a high-affinity inhibitor and hematopoietic prostaglandin D synthase complex by interaction energy studies. *Bioorg Med Chem*. 2018;26(16):4726–4734. https://doi.org/10.1016/j.bmc.2018.08.014.
16 VanDeusen, C.L., Weiberth, F. J., Gill, H.S. et al. Phenyloxadiazole derivatives as PGD inhibitors and their preparation, pharmaceutical compositions and use in the treatment of allergic and inflammatory disorders. WO2011044307, 2011.
17 Weiberth Franz J, Yu Yong, Subotkowski Witold, Pemberton Clive. Demonstration on pilot-plant scale of the utility of 1,5,7-triazabicyclo[4.4.0]dec-5-ene (TBD) as a catalyst in the efficient amidation of an unactivated methyl ester. *Org Process Res Dev*. 2012;16(12):1967–1969. https://doi.org/10.1021/op300210j.
18 Endres G.W., Lee P.H., Olson K.L. et al. Multiheteroaryl compounds as inhibitors of H-PGDS and their use for treating prostaglandin D2 mediated diseases. US 2013/0079375 A1, 2013.